Seismic Retrofit of Framed Buildings Using Self-Centering PC Frames

Mohamed Nour Eldin[1]; Assefa Jonathan Dereje[2]; and Jinkoo Kim[3]

Abstract: In this study, self-centering post-tensioned precast concrete (PC) frames are developed for seismic retrofit of reinforced concrete (RC) framed structures. The cyclic loading test of a RC frame retrofitted with a SC-PC frame is carried out to evaluate the effectiveness of the seismic retrofit. SC-PC frames are applied analytically for the seismic retrofit of three different reinforced concrete model structures using a simple design procedure based on the capacity spectrum method. The effectiveness of the retrofit scheme is investigated through nonlinear time-history response analysis (NLTHA), incremental dynamic analysis (IDA), and seismic fragility analysis. The analysis results indicate that the SC-PC frames are effective in reducing the maximum interstory drift ratio (MIDR) and eliminating the residual drift of the model structures. In addition, the proposed retrofit scheme is effective in increasing the median collapse capacities and decreasing the probabilities of reaching the design limit states of the RC structures. **DOI: 10.1061/(ASCE)ST.1943-541X.0002786.** *© 2020 American Society of Civil Engineers.*

Author keywords: Seismic retrofit; Self-centering; Precast concrete; Post-tension; Fragility analysis.

Introduction

Structural reinforcement plays a key role in mitigating the seismic vulnerability of existing structures not designed for seismic loads. To this end, various seismic retrofit devices have been applied to enhance the seismic safety of structures (Whittaker et al. 1991; Kim and Bang 2003; Lee et al. 2008; Kim et al. 2009; Eldin et al. 2018). Recently, seismic resilience started to attract the attention of many researchers, building owners, and decision makers (Wiebe and Christopoulos 2014; Bocchini et al. 2014; Hutt et al. 2016). Seismic resilience can be measured through the recovering capacity of structures and their ability to resume their functions immediately after an earthquake. In this sense, self-centering systems proved their effectiveness in improving seismic resilience by reducing damage and eliminating residual drift (Guerrini et al. 2008; Palermo and Pampanin 2008). One of the pioneer research projects of concrete self-centering frames came out of the PRESSS (precast concrete seismic structural systems) project during the 1990s (Priestley 1991, 1996; Priestley et al. 1999). Some studies (e.g., Englekirk et al. 2002; Buchanan et al. 2011) indicated that self-centering concrete frames performed well in laboratory seismic testing to limit damage to the structure. Guo et al. (2015) and Song et al. (2015) investigated the seismic performance of a self-centering steel moment-resisting frame with web friction devices and a frame subassembly by conducting a series of experimental tests and a numerical analysis. The results indicated superior performance of the retrofit system against earthquakes. Guo et al. (2016) conducted large-scale experimental investigations of half-scale two-bay self-centering (SC) RC frame systems and conventional RC frame systems. One of the SC systems comprises a reinforced column base, and the other utilizes a post-tensioned column base. The latter system is observed to sustain negligible residual drifts compared with the former one. Qiu and Zhu (2017) conducted a series of shake table tests on a one-fourth-scaled, two-story, one-bay frame model with shape memory alloy braces and validated the effectiveness of the proposed retrofit system. The results indicated that the self-centering system was able to sustain several strong earthquakes without severe damage, performance deterioration, or permanent deformation of the frame. Dyanati et al. (2017) compared the seismic performance and economic effectiveness of two prototype concentrically braced frame buildings with and without a self-centering system. Based on the life cycle costs and annual probabilities of exceeding various damage levels, the results indicated that the self-centering system caused lower drift-related losses but higher acceleration-related losses for the buildings.

Most previous studies related to self-centering systems are dedicated to new structures because including the SC system in new buildings is easier. In contrast, few studies are applied to retrofit or upgrade existing structures using an SC system. Among these few studies, Guo et al. (2017) proposed a seismic retrofit technique for an RC-framed building in a high seismic zone using a self-centering concrete wall with friction dampers. In situ vibration tests were conducted to validate the retrofit technique. The proposed self-centering walls succeeded in increasing the lateral deformation capacity and reducing the residual drift of a five-story building such that the building can be used after a major earthquake. Naeem and Kim (2018b) investigated the effectiveness of damped cable systems (DCS), which uses additional stiffness and damping combined with the self-centering system. Their study indicated that fewer damper units were required for the case of the DCS, and the seismic fragility was less compared with the VD technique. Naeem and Kim (2018a) carried out shaking table tests of a two-story steel frame installed with the proposed damping system and demonstrated that the proposed damping system with added stiffness and self-centering

[1]Assistant Professor, Dept. of Civil and Architectural Engineering, Sungkyunkwan Univ., Suwon 16419, Republic of Korea.

[2]Graduate Student, Dept. of Civil and Architectural Engineering, Sungkyunkwan Univ., Suwon 16419, Republic of Korea.

[3]Professor, Dept. of Civil and Architectural Engineering, Sungkyunkwan Univ., Suwon 16419, Republic of Korea (corresponding author). ORCID: https://orcid.org/0000-0002-3605-8189. Email: jkim12@skku.edu

Note. This manuscript was submitted on February 27, 2019; approved on April 29, 2020; published online on July 24, 2020. Discussion period open until December 24, 2020; separate discussions must be submitted for individual papers. This paper is part of the ***Journal of Structural Engineering***, © ASCE, ISSN 0733-9445.

capability is effective in reducing earthquake-induced displacement and member forces. Huang et al. (2018) investigated the effect of different types of infill walls (IW) on retrofit bare self-centering prestressed concrete frames (SCPC) with beam-web friction devices. The nonlinear static and dynamic analyses indicated that SCPC-IW was effective in decreasing the lateral displacement; however, the residual deformation and axial compression ratio of the SCPC-IW system increased. The study revealed that the optimum range of the ratio between the load capacity of infill walls and web friction force should be between 0.37 and 0.79 to achieve a good balance in terms of stiffness, energy dissipation, and self-centering capability, as well as collapse resistance capability for the retrofitted system. Nour Eldin et al. (2019) proposed a retrofit design procedure for existing structures using self-centering post-tensioned precast concrete (PC) frames utilizing the initial stiffness and the N2 method. The SC-PC frame is considered an easy and practical option compared with the traditional cast-in-situ concrete frames (Bahrami et al. 2017; Morgen and Kurama 2008). SC-PC frames are characterized by their recentering capacity developed by unbonded post-tensioned tendons. In this study, the seismic performance of SC-PC frames is evaluated by both experimental and numerical studies. Two experimental quasi-static (cyclic) tests are applied on a one-story RC frame before and after retrofit with the SC-PC frame to validate the proposed retrofit scheme. For numerical study, SC-PC frames are applied to the seismic retrofit of RC analysis model structures, and the retrofit effectiveness is assessed by nonlinear dynamic analyses. A simple design procedure for SC-PC frames is developed using the capacity spectrum method (CSM). To predict the collapse capacity of the case study structures before and after the retrofit, an incremental dynamic analysis (IDA) was conducted using different sets of ground motions scaled to increasing intensity levels. In addition, the probabilities of reaching different damage limit states are investigated through seismic fragility analyses.

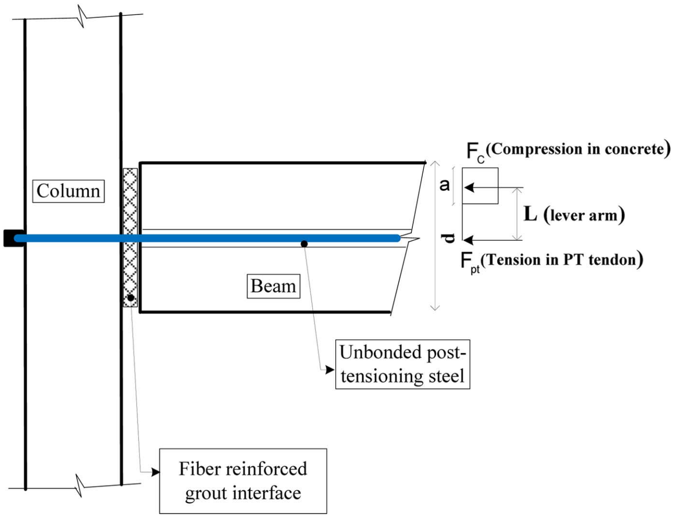

Fig. 1. Beam-column interface of SC-PC retrofit frame.

Analytical Modeling of SC-PC Retrofit Frame

The stress-strain relation of the post-tensioning tendon recommended by Mattock (1979) for Grade 270 prestressing strands is given by Eq. (1)

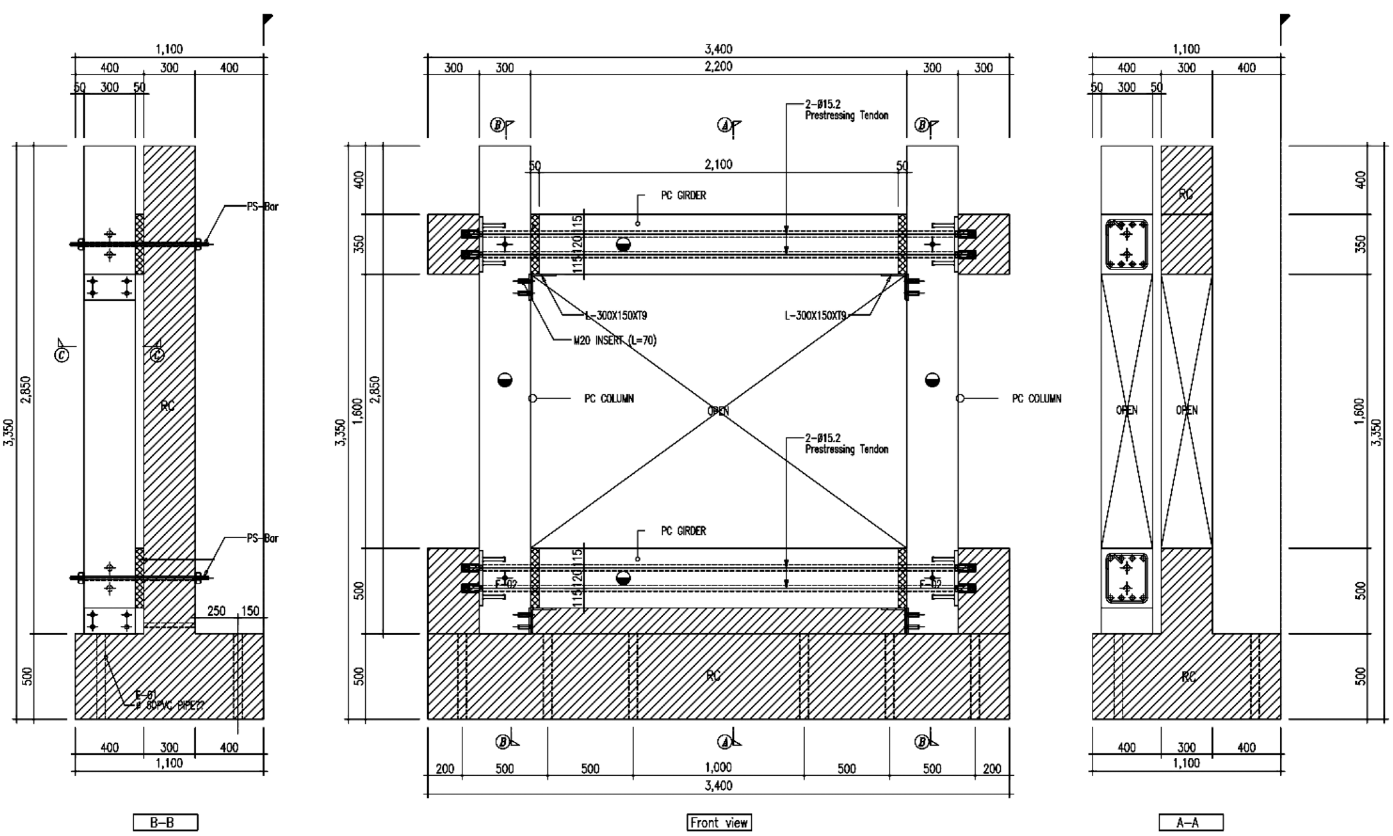

Fig. 2. SC-PC retrofit frame attached to RC frame for the experiment.

$$f_{pt} = \varepsilon_{pt} \cdot E_p \cdot \left[0.02 + 0.98 \Big/ \left[1 + \left(\frac{\varepsilon_{pt} \cdot E_p}{1.04 \cdot f_{py}}\right)^{8.36}\right]^{1/8.36}\right] \quad (1)$$

where f_{pt} and ε_{pt} = stress and strain in the post-tensioning tendon; E_p = elastic modulus of the prestressing steel; and f_{py} = yield strength of the post-tensioning tendon.

The moment capacity of the beam-column connection, M_{cap}, is calculated by multiplying the force developed in the post-tensioning tendon, F_{pt}, with the distance to the resultant concrete compression force, F_c, as indicated in Fig. 1. From equilibrium

$$F_c = F_{pt} \quad (2)$$

Then, the internal moment of the beam-column connection is obtained as follows:

$$M_{int} = F_{pt} \cdot (h_g - a)/2 \quad (3)$$

where h_g = height of the grout pad at the beam-column interface; and a = depth of the equivalent rectangular compression stress block corresponding to the compression force, which can be determined using the following equation [ACI-318 (ACI 2014)]:

$$a = F_c / 0.85 f'_c b_g \quad (4)$$

where F_c = concrete compression force; b_g = width of the grout pad at the beam-column interface; and f'_c = unconfined concrete compression strength. At the yield of the post-tensioning tendon, the moment capacity M_{cap} can be calculated as

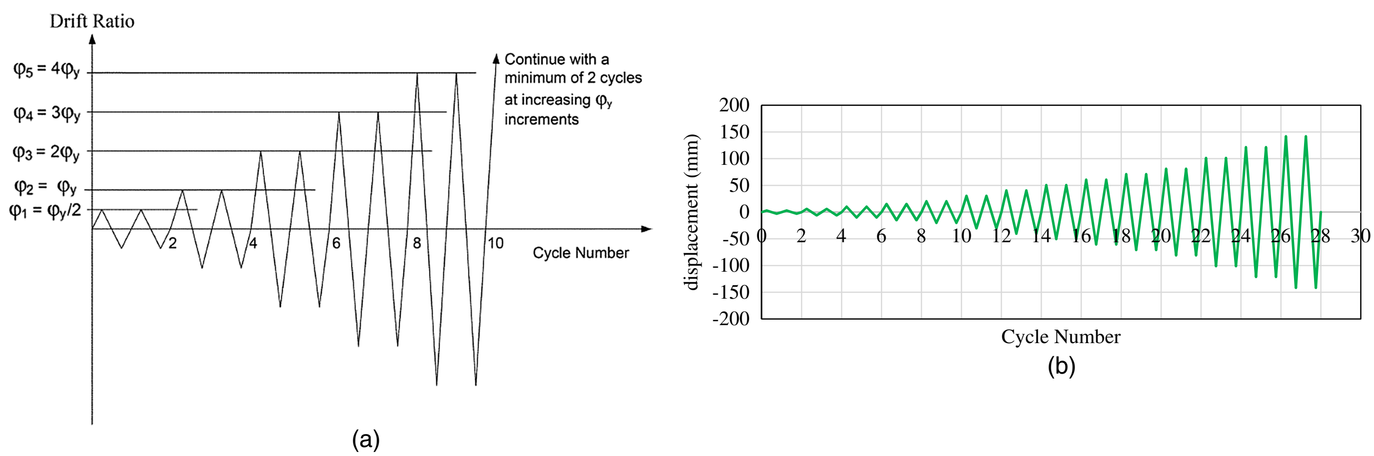

Fig. 3. Loading protocol: (a) ACI 374.2r-13; and (b) applied loading protocol.

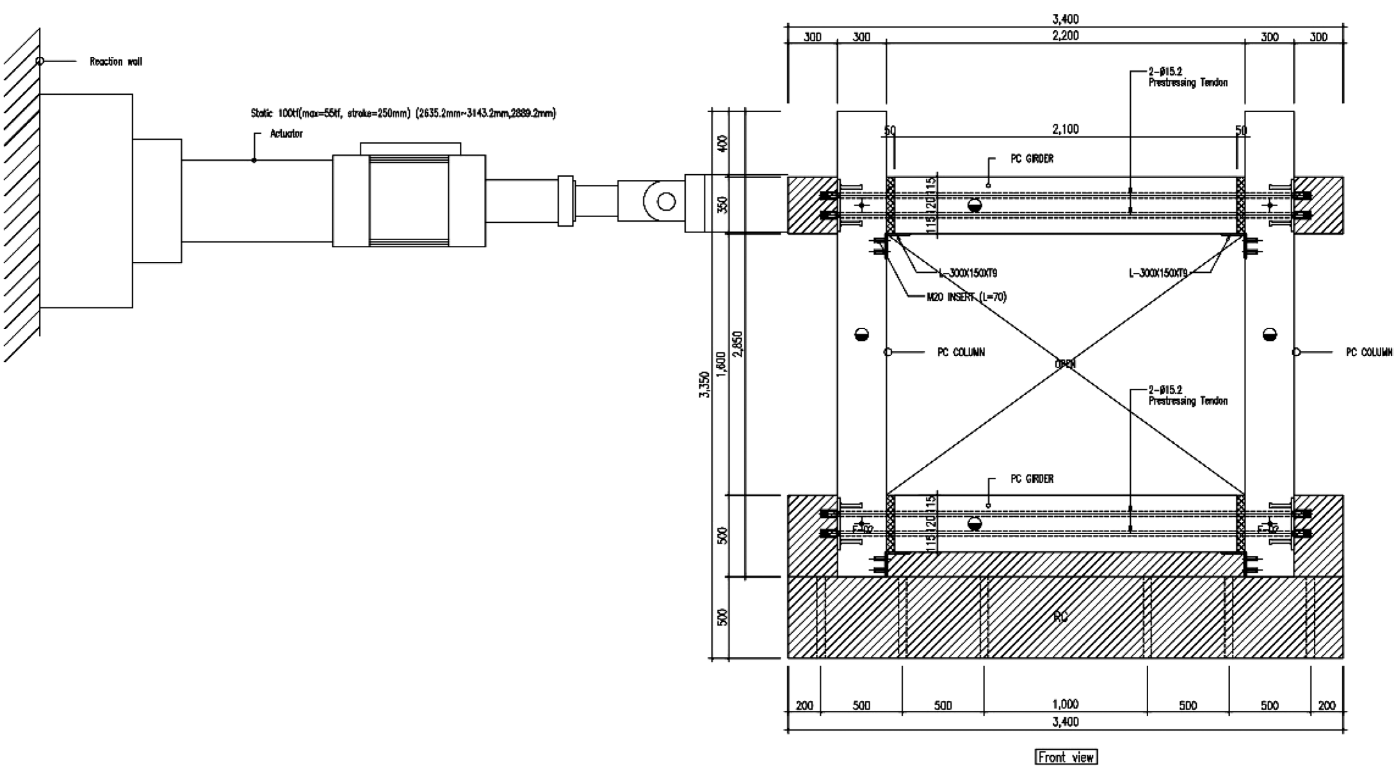

Fig. 4. Cyclic loading test setup.

J. Struct. Eng., 2020, 146(10): 04020208

RC frame specimen with the foundation setup for the test

RC and SC-PC frame specimens before the test and during the test

Vertical steel towers are used to prevent out of plane movement during the test

The anchor bolts connecting the frames and the tendons setup before the test

Fig. 5. SC-PC frame attached to PC frame.

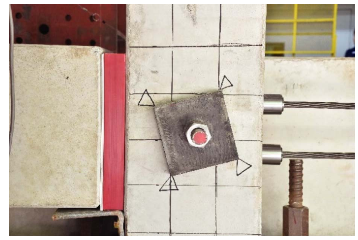

Teflon and thin steel plates are used between the beam and column of the PC frame.

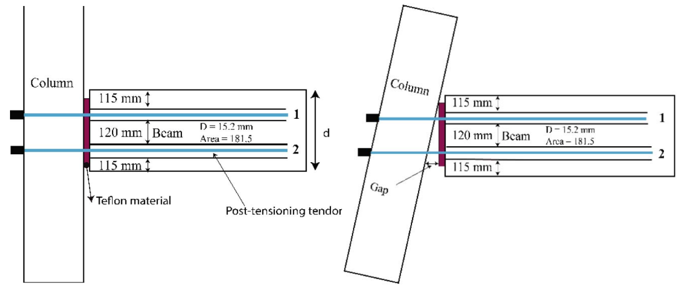

Schematic drawing of the SC-PC beam-column interface before and after gap opening

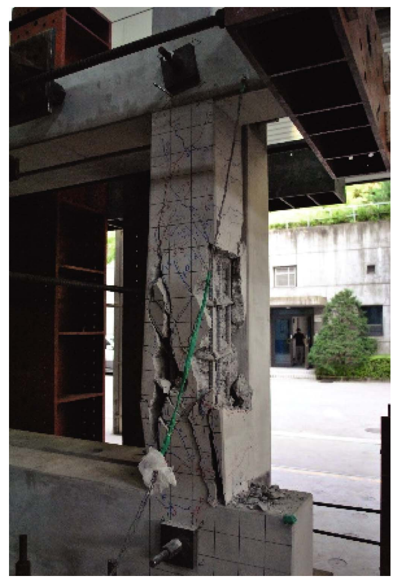

The RC frame damage state after the test

Fig. 5. (*Continued.*)

$$M_{cap} = F_{py} \cdot (h_g - a)/2 \tag{5}$$

The decompression point defines the beginning of a gap opening at the connection interface and corresponds to the condition for which the stress in the extreme concrete compression fiber reaches zero at the beam-end. Accounting for the precompression introduced by the initial prestressing force and assuming a linear strain distribution at the critical section, the following equation is used to determine the moment resistance at the gap opening, M_{decomp} (Celik and Sritharan 2004)

$$M_{\mathrm{decomp}} = \sigma_i \cdot I \Big/ \left(\frac{h_g}{2}\right) \tag{6}$$

where σ_i = stress in the beam from initial prestressing; I = moment of inertia of the beam section based on the gross section properties; and h_g = height of the grout pad at the interface. At the beam-column interface, a bilinear elastic spring is used where the gap

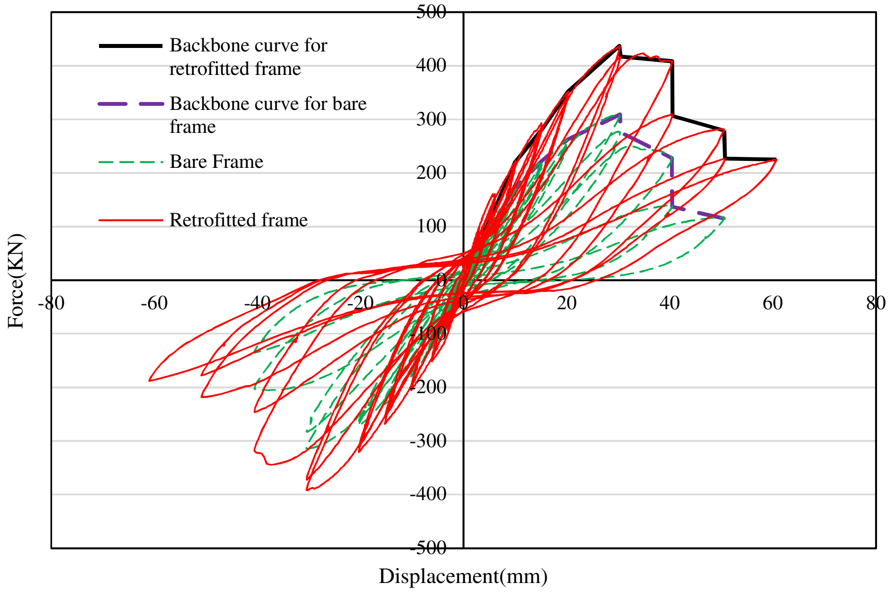

Fig. 6. Hysteresis curves of RC frame before and after retrofit.

opening starts between the column and the beam at the decompression level in the PT tendons. When the applied moment exceeds M_{decomp}, the gap increases and the PT tendons start to elongate.

Configuration of Test Frame Specimen

Seismic retrofit of an existing RC structure at the outside of the building is more practical because it will not stop the function of the building during the retrofit, and there is more flexibility in the attachment of the retrofit elements. In the present study, an SC-PC frame is added to the outer perimeter of an RC frame for a seismic retrofit, and the seismic retrofit effect is evaluated using a cyclic loading test. Fig. 2 indicates the SC-PC frame attached to the RC frame before the start of the experiment. The column and beam cross-section dimensions of the RC frame are 300 × 300 and 300 × 350 mm, respectively. The columns are reinforced with eight D22 main rebars with D10 stirrups spaced 200 mm apart. The beam's main reinforcement is eight D22 rebars (four each at the top and bottom) with D10 stirrups every 150 mm.

The overall dimensions of the SC-PC column and beam are 300 × 300 × 2,850 and 300 × 350 × 2,100 mm, respectively. The PC beams are located at the top and bottom of the PC columns. A 50.0 mm Teflon plate is inserted at the interface between the beams and columns. Steel seat angels are used for positioning beams during the erection and pretensioning of the PT tendons. The main column reinforcement of the PC column is twelve D22 bars with D10 stirrups every 200 mm. The reinforcement of the PC beam consists of six D22 main rebars (three top and bottom) with D10 stirrups every 150 mm.

The prestressing seven-wired tendon (diameter of 15.2 mm) has a yield strength of 1,600 MPa and 146 kN pretensioning force. The concrete compressive strengths for RC and PC frames are 22 and 40 MPa, respectively. The rebar yield strength for RC and PC frames are 400 and 500 MPa, respectively. The SC-PC frame is connected to the RC frame through horizontal anchor bolts (diameter 32.0 mm and yield strength of 930 MPa) that connect the two frames at the connection between the beam and column, as indicated in Fig. 2. These anchor bolts are designed based on the maximum horizontal force that will be transferred from the RC frame to the SC-PC frame through shear stresses in the anchors. The AISC-360 (AISC 2016) procedure for the shear design of anchor bolts is used to obtain the diameter of the anchor bolts. For dynamic loading, the design force is the inertia-force induced at the floor level. For a quasi-static test, the design force can be the maximum strength obtained from the analytical pushover curve of the RC and PC frame assembly. The connecting anchors are designed primarily to have sufficient stiffness and strength to remain elastic during the experiment. The main role of these anchors is to transfer the horizontal loads from the RC frame to the PC frame at the floor level, and 50.0-mm-thick Teflon plates are used at the interface of the RC and PC frames to prevent any friction between the frames. The PC frame is resting on the foundation of the RC frame.

Cyclic Loading Test of Test Specimens

Displacement-controlled cyclic tests of the specimens are carried out using a 2,000-kN hydraulic servo actuator to evaluate their seismic performance. Strain gauges are attached to the steel reinforcement bars of the RC frame at different locations. LVDTs are installed to measure the horizontal displacement at the upper part of the specimens during the loading test. Fig. 3 indicates the displacement history used for the test, which is constructed based on the loading protocol for quasi-static cyclic tests specified in ACI 374.2r-13 (ACI 2013). At the beginning of the loading, the displacement amplitude is doubled in every two cycles; subsequently,

Table 1. Gap angles at different stages of global lateral displacement of system

Global lateral displacement (mm)	Gap angle (rad)
10.0	0.004
20.0	0.008
30.0	0.012
40.0	0.016
50.0	0.020
60.0	0.024

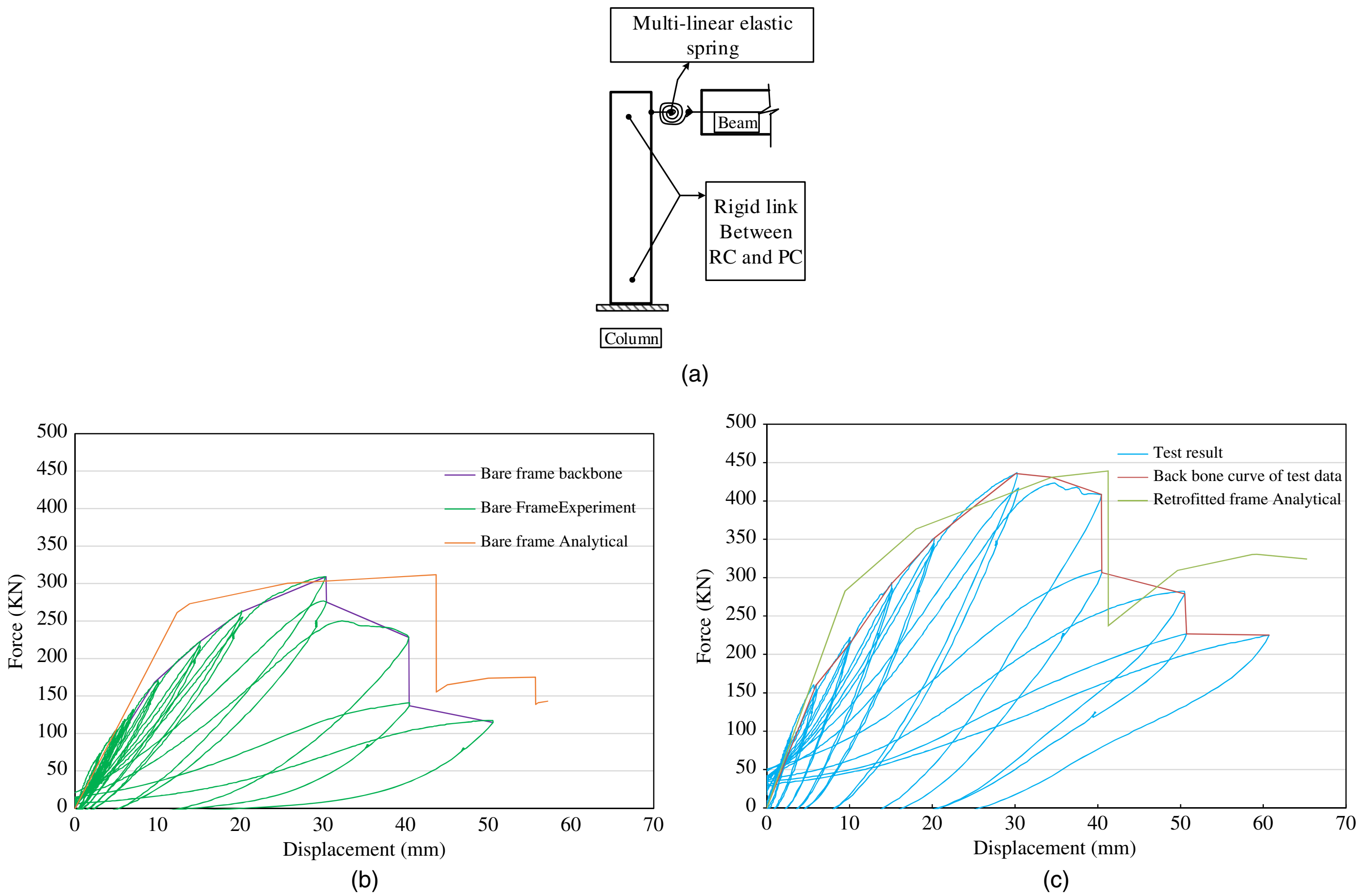

Fig. 7. Numerical and experimental backbone curves of RC frame: (a) analytical modeling of SC-PC frame; (b) backbone curve before retrofit; and (c) backbone curve after retrofit.

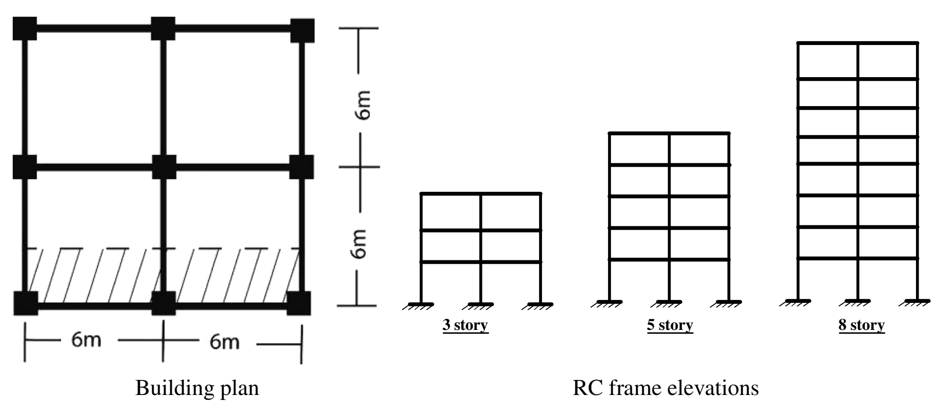

Fig. 8. Plan and elevations of RC frames.

Table 2. Reinforcement details of beams of model structures

Categories		Values
Model		3, 5, and 8-story
Dimensions (mm)		250 × 400
Longitudinal reinforcement	Top	4 D20
	Bottom	4 D20
Transverse		D8@150 mm

Table 3. Reinforcement details of columns of model structures

Model	Dimensions (mm)	Longitudinal reinforcement	Transverse
3-story	300 × 300	6 D14	D8@150 mm
5-story	400 × 400	8 D16	
8-story	450 × 450	12 D16	

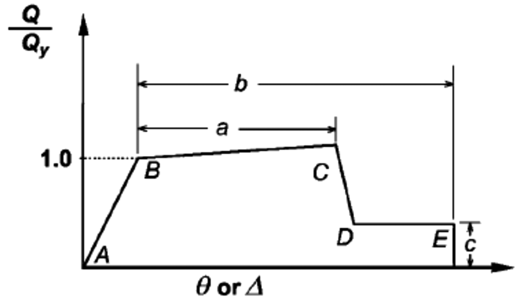

Fig. 9. Generalized force-deformation relationship of RC beams and columns.

the increase in amplitude is maintained as a multiple of the yield drift of the frame.

Fig. 4 indicates the setup of the cyclic loading test. The hydraulic actuator is fixed to a stiff concrete reaction wall and is connected to a data acquisition system to plot a real-time force-displacement relation of the actuator. Fig. 5 indicates the bare and retrofitted RC frame specimens. A 50-mm thick Teflon plate is used with thin steel plates to make the horizontal precast beam fit during the assembly of the SC-PC frame to assure complete contact between the beam and column of the PC frame. A steel plate is used for the anchor bolt to avoid concentration of excessive pressure on the concrete surface during the test. The damage pattern of the RC frame specimen is indicated in Fig. 5.

Fig. 6 indicates the hysteresis curves of the RC frame before and after retrofit obtained from the experiment. As can be observed from Fig. 6, the initial stiffness of the frame is significantly increased after the retrofit. In addition, the total strength of the retrofitted frame is higher than the unretrofitted one by almost 40%. The first drop of the resistance of the frame started at a lateral displacement of almost 30.0 mm, which is an approximately 1.5% interstory drift of the RC frame specimen. The RC frame is observed to reach the total collapse at a lateral displacement of 50.0 mm (i.e., IDR = 2.5%), whereas the retrofitted frame reaches total collapse at 60.0 mm (IDR = 3.0%). The total collapse is defined as the state at which the lateral load resisting capability of the specimens drop significantly (below 40% of the maximum strength). Table 1 indicates the theoretical gap angles at different stages of the global lateral displacement of the system. The stress-strain relationship of the post-tensioned (PT) tendon remains in the elastic range during the experiment. The PT tendon stress is computed to reach as high as 1,300 MPa, and the corresponding strain reaches 0.008 during the test.

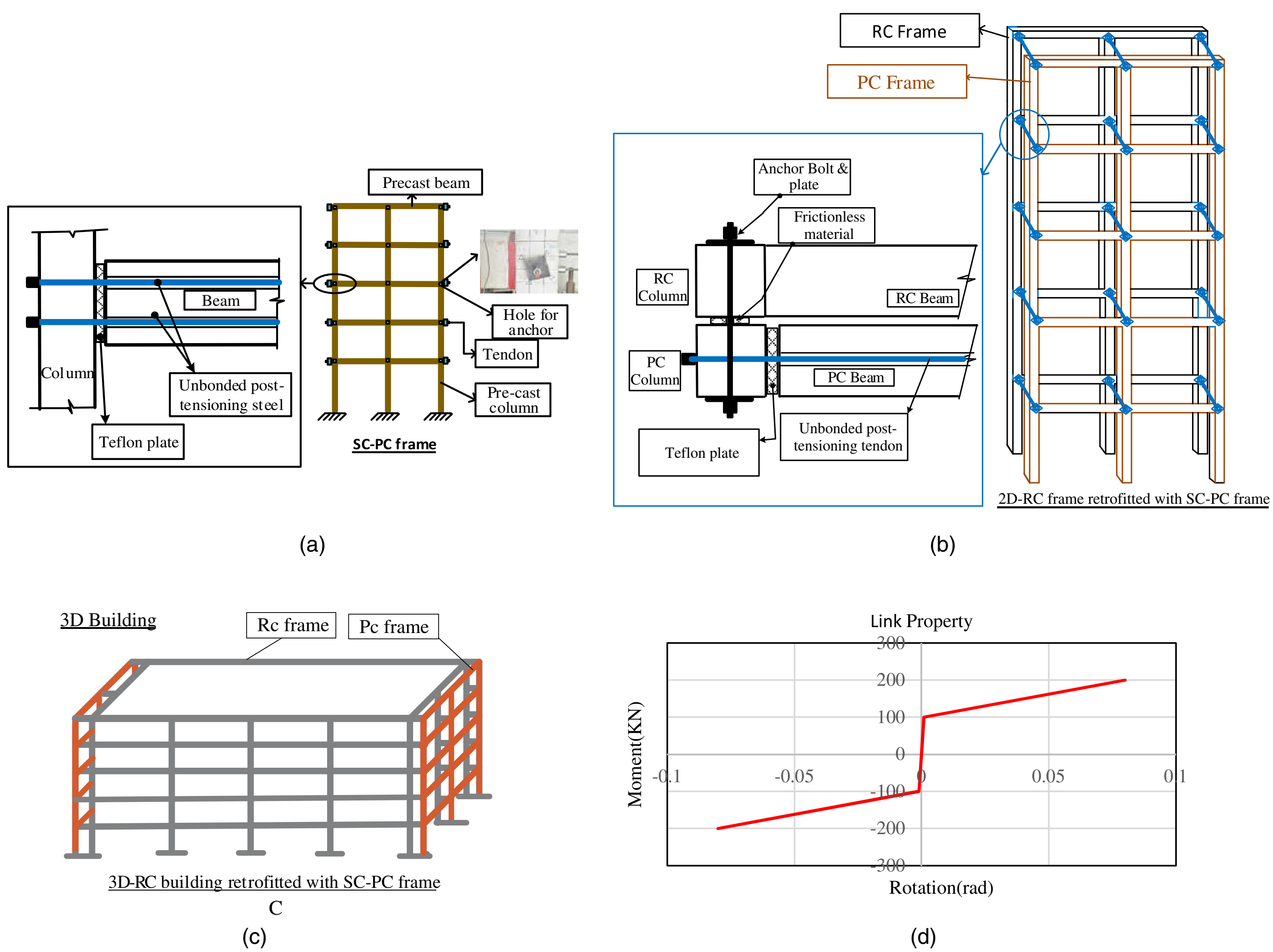

Fig. 10. SC-PC frame and its attachment to RC frame: (a) SC-PC frame; (b) 2D-RC frame; (c) 3D-RC frame; and (d) multilinear elastic link.

Fig. 7 provides a comparison between the numerical and experimental backbone curves of the RC frame before and after the retrofit. SAP2000 (2018) software is used to numerically obtain the specimen backbone curve. The analytical modeling of the PC frame is indicated in the same figure. A multilinear spring is used from the SAP2000 library to model the connection between the beam and column of the PC frame. A rigid link is used to model the anchor bolt that connects the RC and PC frames. Frame elements in SAP2000 are used to model the RC beams and columns considering the longitudinal and shear reinforcement. Plastic hinges are assigned at the ends of the RC beams and columns to account for the nonlinear behavior. The parameters of the plastic hinges are determined from the recommendations of ASCE/SEI-41 (ASCE 2013). As is observed in Fig. 7, the initial stiffness predicted by the numerical model coincides well with the stiffness obtained from the experiment. Although both the numerical and experimental curves indicate the same maximum strength, the numerical backbone curves generally display a distinct yield point, whereas the experimental ones display a smooth transition. The numerical backbone curve of the unretrofitted RC frame drops at a lateral displacement of 43.0 mm with an abrupt change in strength. Meanwhile, the experimental curve indicates the first drop in resistance at the lateral drift of 30.0 mm, followed by a stepwise degradation in strength. Generally, the numerical and experimental backbone curves match better in the retrofitted frame than in the unretrofitted frame with some difference after a major drop in resistance at around a 40.0-mm lateral displacement. The differences between the numerical and experimental results can be attributed primarily

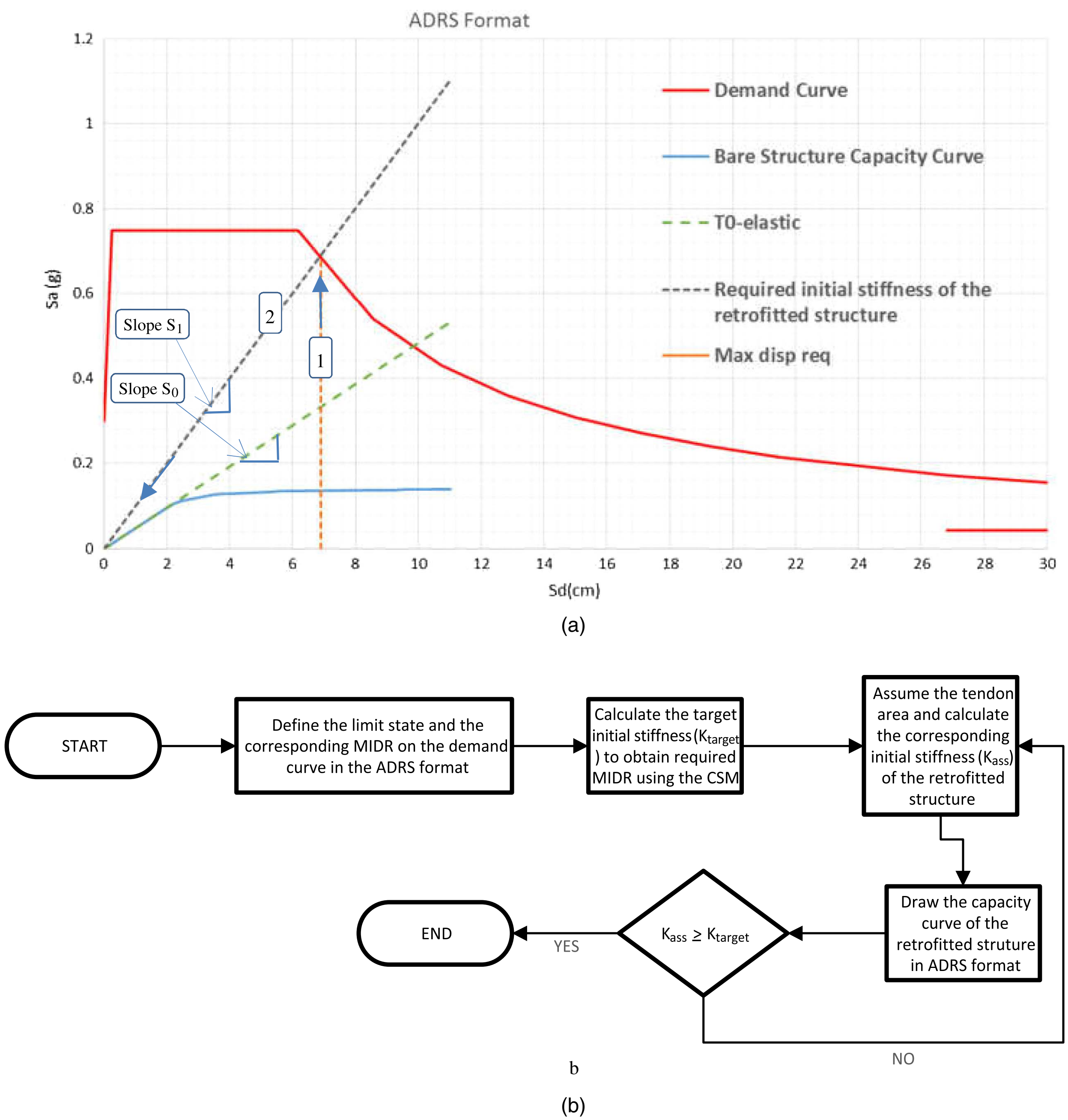

Fig. 11. Proposed seismic retrofit procedure: (a) demand and capacity curves of bare structure on ADRS format and required stiffness of retrofitted structure; and (b) flowchart of procedure for obtaining required tendon area.

to the disability of the numerical model in predicting crack formations during the loading and unloading process.

Seismic Retrofit of RC Structures with SC-PC Frames

In this section, a seismic evaluation of analysis model structures retrofitted with the SC-PC frame is conducted to verify the effectiveness of the retrofit scheme on enhancing the seismic performance of the structures. Worth mentioning is that a tradeoff exists between increasing the stiffness of the structure and increasing the level of the seismic demand for the same structure when the natural frequency of the model structure is shifted toward the dominant frequency of the earthquakes. The proposed retrofit scheme is intended to increase the overall stiffness of the structure to the point at which the drift demand is maintained within the required limit state. In addition, the residual drift of the original structure is expected to be reduced. In contrast, the demand for the structural components, such as connections, may be increased. Therefore, the proposed retrofit scheme is more suitable for structures with a higher margin of safety at the connection capacity and material strength.

Design and Analytical Modeling of Analysis Model Structure

Fig. 8 indicates the structural plan and elevations of the three-, five-, and eight-story RC analysis model structures. The model structures are designed only for a gravity load combination (1.2D + 1.6L) based on ACI-318 (ACI 2014) without considering the seismic provisions. The gravity load comprises a dead load of 4.1 kN/m^2 and a live load of 2.5 kN/m^2. The RC frame structures have beam sections of 250×400 mm. Square column sections with dimensions of 300, 400, and 450 mm are used for the three-, five-, and eight-story frames, respectively. Four D20 longitudinal reinforcement bars are used at the top and bottom of the beam. Six D14 longitudinal reinforcement bars are used for the three-story RC-frame column reinforcement. Eight and twelve D16 longitudinal reinforcement bars are used for the column reinforcement of the five- and eight-story frames, respectively. Both beams and columns have D8@150 mm transverse reinforcement in all frames (Tables 2 and 3). The compressive strength of the concrete is taken as 20.7 MPa (3,000 psi), and grade 60 (413 MPa yield strength) steel is used for the reinforcement bars.

The RC sections are assumed to be in cracked conditions, and the moment of inertia of the beam and the column sections are reduced to 35% and 70% of those of nominal uncracked values, respectively. Modal damping of 5% of the critical damping is used in the analyses, and material nonlinearity is accounted for by defining localized plastic hinges at the ends of the structural elements. After conducting a modal analysis of the RC frames, the fundamental periods of the three-, five-, and eight-story frames are found to be 0.87, 1.2, and 1.9 s, respectively.

The analysis model for the beam elements of the RC frame is composed of two end rotation type moment hinges defined using ASCE/SEI 41-13 (ASCE 2013). Fig. 9 indicates the generalized force-deformation relationship for RC beams and columns used in the dynamic analysis. In Fig. 9, the vertical axis represents the ratio between the applied action (force or moment, Q) and the yield value, Q_y, and the horizontal axis represents the deformation (rotation angle, θ, or displacement, Δ). The parameters a and b refer to deformation portions that occur after yield, or plastic deformation. The parameter c is the reduced resistance after a sudden reduction from C to D. Parameters a, b, and c are defined numerically in Tables 10-7 and 10-8 in ASCE-41 (ASCE 2013). These parameters are automatically calculated for each section using SAP2000 version 20 and depend on the reinforcement ratio, shear force, and axial force of the section under consideration. The nonlinear static analysis required for the proposed procedure is performed using SAP2000 software. Columns are fixed at the base, and all columns and beams are rigidly connected. Member elements in the software library are used to model the beams and columns. Fig. 10 indicates the SC-PC frame and its attachment to the RC frame. For the SC-PC frame, the beams are modeled as member elements with a multilinear elastic link at both ends of the beams, as indicated in Fig. 10. Columns are modeled as member elements and are fixed at the base.

Proposed Design Procedure for SC-PC Frame

In this section, a simplified seismic retrofit design procedure of the SC-PC frame is presented. The seismic retrofit of an existing structure is not an easy task, especially when the retrofit requires stopping the function of the structure during construction. The proposed external retrofit scheme using the SC-PC frame can minimize the loss time needed for retrofit. Worth mentioning is that the proposed procedure depends primarily on modifying the elastic stiffness of the main lateral resisting system of the existing building using the SC-PC frames on the basis of a prescribed drift limit state (for example, the maximum interstory drift ratio (MIDR) of 1.0%, which corresponds to the limit state for important buildings subjected to design basis earthquakes). The additional stiffness added by the SC-PC frames is calculated to achieve this target MIDR using ADRS (acceleration-displacement response spectra) of the structure.

To determine the added stiffness required to satisfy the given performance limit state, the capacity spectrum method (CSM) specified in the ATC-40 (ATC 1996) is applied. The CSM is applied to obtain the performance point in each case in which the stiffness is modified to the K_{target}. The strength and the secant stiffness are considered in the CSM procedure to obtain the required maximum interstory drift (MIDR). Based on that, strength, secant stiffness, and ductility of the retrofitted system are considered to obtain the highly damped demand spectrum and the required MIDR. To this end, nonlinear static pushover analysis of the model structure is carried out using a lateral load proportional to the fundamental mode shapes. Fig. 11 provides a sample of the demand and capacity curves of the bare structure on the ADRS format and a simple flowchart of the design procedure used to obtain the required tendon cross-sectional area to be inserted in the PC beams. The required initial stiffness of the retrofitted frame can be determined, as indicated in the graph, and

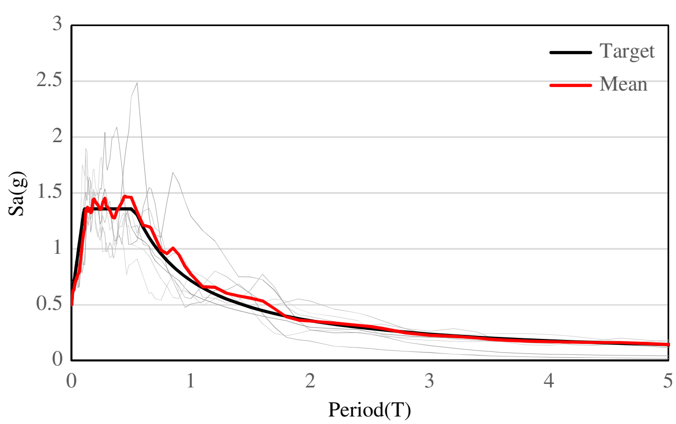

Fig. 12. Target design spectrum and response spectra of seven earthquakes.

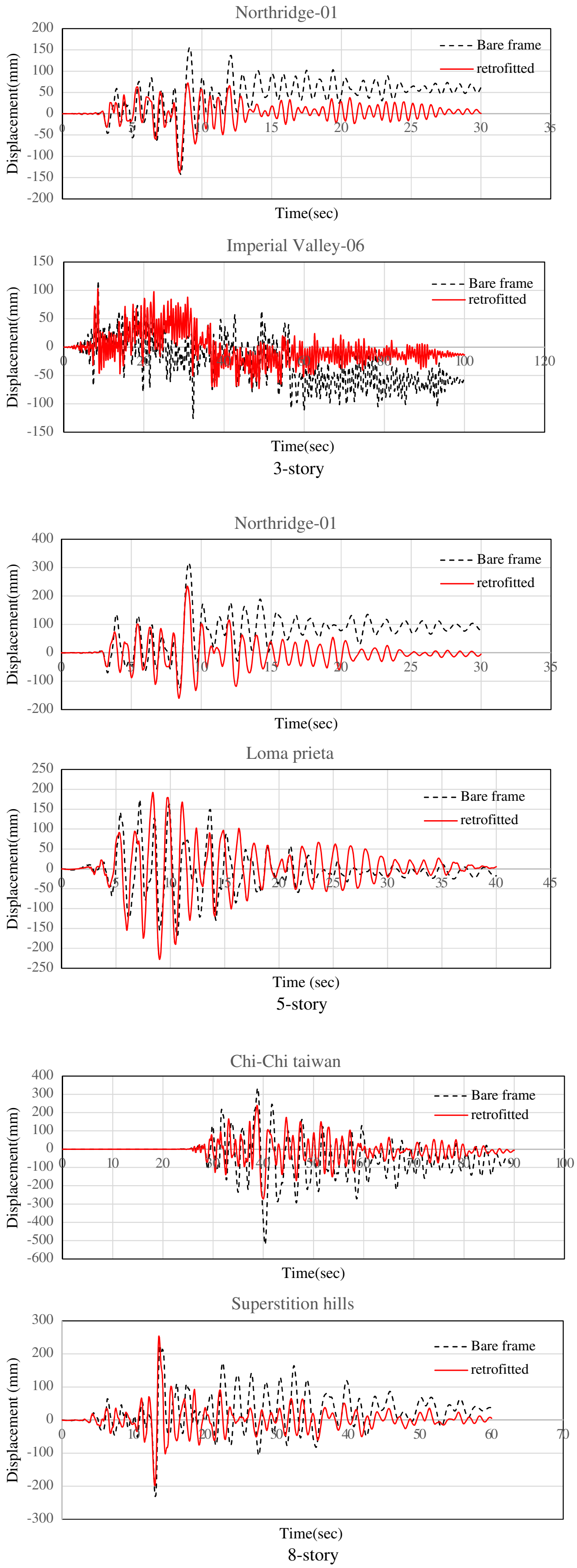

Fig. 13. Roof displacement time-history of three-, five-, and eight-story frame structures before and after retrofit.

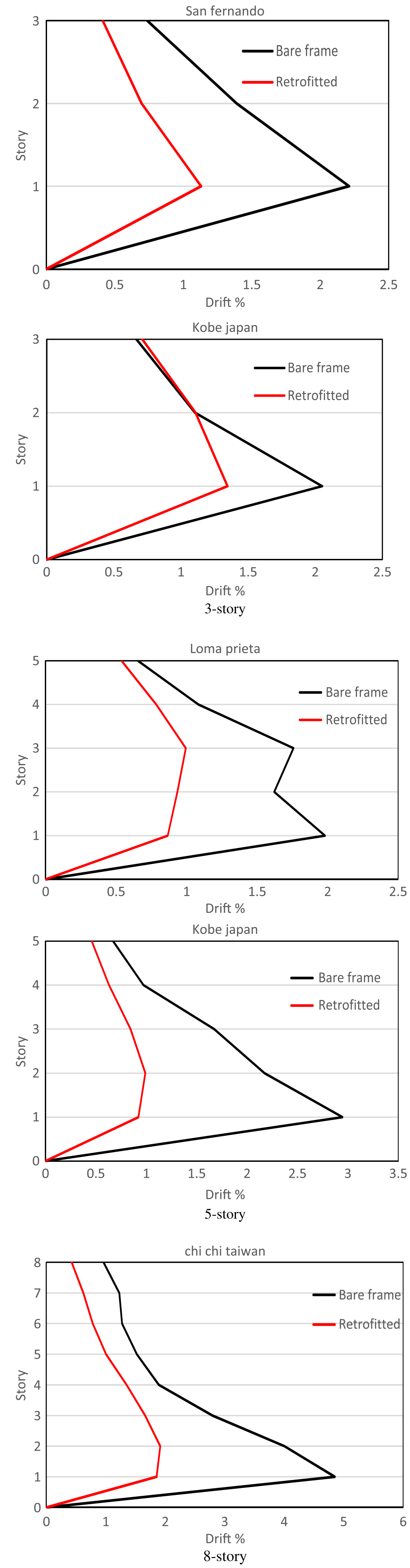

Fig. 14. MIDR of three-, five-, and eight-story frame structures before and after retrofit.

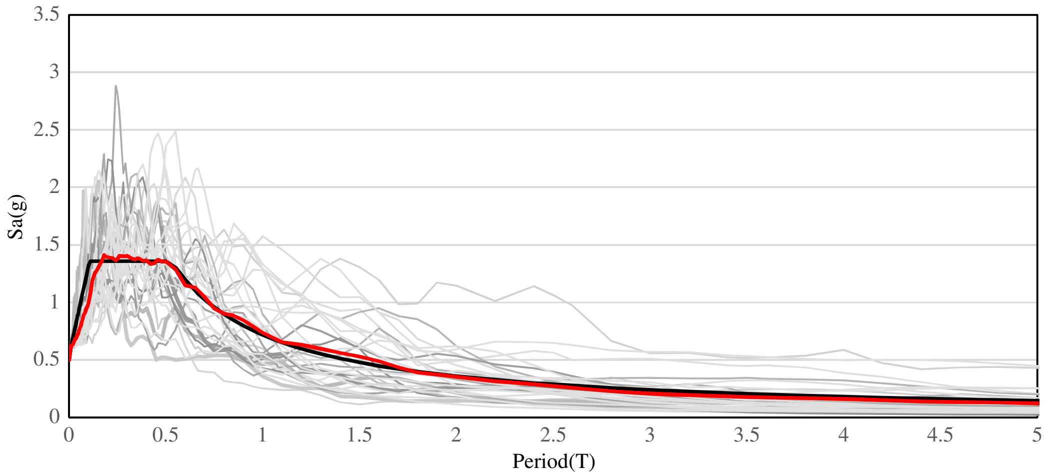

Fig. 15. Response spectra of ground motion records used for IDA.

the difference between the initial stiffness before and after retrofit is the required SC-PC frame stiffness. The structure is assumed to be dominated by the fundamental vibration mode, and the equal displacement rule is applicable. Assuming that the same area of the tendon is used at each story level, a simple trial and error approach is used to obtain the area of the tendon that provides the required stiffness of the SC-PC frame. Because the dimensions of the SC-PC beam and column are assumed to be the same as that of the RC frame, the only variable for this trial and error approach is the total cross-sectional area of the tendons.

For the present study, the yield strength of the post-tensioning tendons, f_{py}, and the initial stress after losses, f_{pi}, are assumed to be 1,600 and 820 MPa, respectively, and the nominal compressive concrete strength, f'_c, is 20.7 MPa. Two tendons are used in each beam, as in the experiment. The retrofit frame is rigidly connected to the bare frame at each floor level to maintain a rigid diaphragm. Guidelines for such a connection are provided elsewhere (e.g., Rahman and Sritharan 2007).

Nonlinear Dynamic Response Analysis Results

In this section, the seismic performances of the model structures before and after the seismic retrofit are evaluated using nonlinear time history (NLTH) analysis. The case study structures are assumed to be located in the site class SD soil profile with the spectral acceleration coefficients of $S_{DS} = 0.70$ g and $S_{D1} = 0.38$ g using the ASCE 7-16 (ASCE 2016) format. Nonlinear dynamic analysis-based seismic performance assessment is carried out using seven earthquake records scaled to the design spectrum. Fig. 12 provides the design spectrum and response spectra of the seven scaled earthquakes.

Fig. 13 provides the roof displacement time histories of the three-, five-, and eight-story structures for some selected earthquakes. As observed in Fig. 13, the maximum roof displacements decrease after the seismic retrofit. In addition, the residual drift was eliminated relative to the unretrofitted case for these selected records. Fig. 14 provides the maximum interstory drift ratios (MIDR) of the model structures obtained from the nonlinear dynamic analyses. The MIDR is observed to be reduced significantly after the retrofit of the structures. For the five-story structure, the retrofit is effective in reducing the MIDR within 1.0% of the story height. For the three- and eight-story models, the MIDR is maintained within 2.0%.

Evaluation of Seismic Collapse Capacity

Nonlinear incremental dynamic analyses (IDA) of the structures before and after the retrofit are conducted using the 30 ground motion records obtained from the PEER NGA Database (PEER 2017) to establish the median and standard deviation of the collapse capacity of each analysis model. Fig. 15 indicates the 30 response spectra of the ground motion records anchored to the peak ground acceleration of the design spectrum, and Table 4 indicates the characteristics of these earthquake records. IDA curves are obtained by conducting NLTH analyses and monotonically increasing the

Table 4. List of earthquake records used in IDA

Earthquake name	PEER code	Station
San Fernando	RSN-68	LA–Hollywood Stor FF
Friuli Italy-01	RSN-125	Tolmezzo
Imperial Valley-06	RSN-169	Delta
Imperial Valley-06	RSN-174	El Centro Array #11
Superstition Hills-02	RSN-721	El Centro Imp. Co. Cent
Superstition Hills-02	RSN-725	Poe Road (temp)
Loma Prieta	RSN-752	Capitola
Loma Prieta	RSN-767	Gilroy Array #3
Cape Mendocino	RSN-828	Petrolia
Landers	RSN-848	Coolwater
Landers	RSN-900	Yermo fire station
Northridge-01	RSN-953	Beverly Hills–14145 Mulhol
Northridge-01	RSN-960	Canyon Country–W Lost Cany
Kobe Japan	RSN-1111	Nishi-Akashi
Kobe Japan	RSN-1116	Shin-Osaka
Kocaeli Turkey	RSN-1148	Arcelik
Kocaeli Turkey	RSN-1158	Duzce
Chi-Chi Taiwan	RSN-1244	CHY101
Chi-Chi Taiwan	RSN-1485	TCU045
Duzce Turkey	RSN-1602	Bolu
Manjil Iran	RSN-1633	Abbar
Hector Mine	RSN-1787	Hector
Kern County	RSN-12	LA-Hollywood Stor FF
El Alamo	RSN-22	El Centro Array #9
Parkfield	RSN-30	Cholame-Shandon Array#5
Borrego Mtn	RSN-38	LB-Terminal island
Friuli Italy 01	RSN-121	Barcis
Gazli USSR	RSN-126	Karakyr
Tabas Iran	RSN-138	Boshrooyeh
Trindad	RSN-280	Rio Dell Overpass–FF

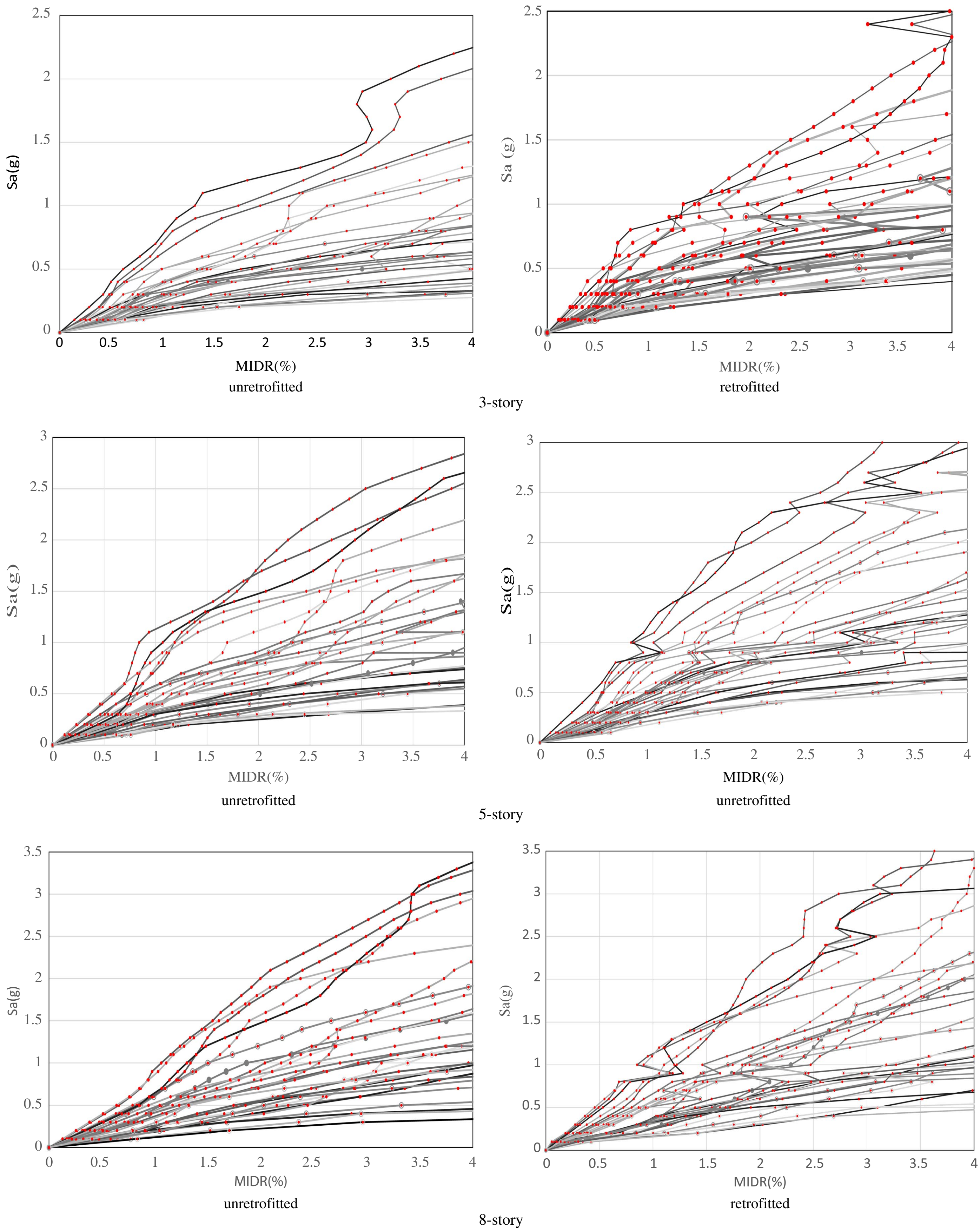

Fig. 16. IDA curves of model structures.

J. Struct. Eng., 2020, 146(10): 04020208

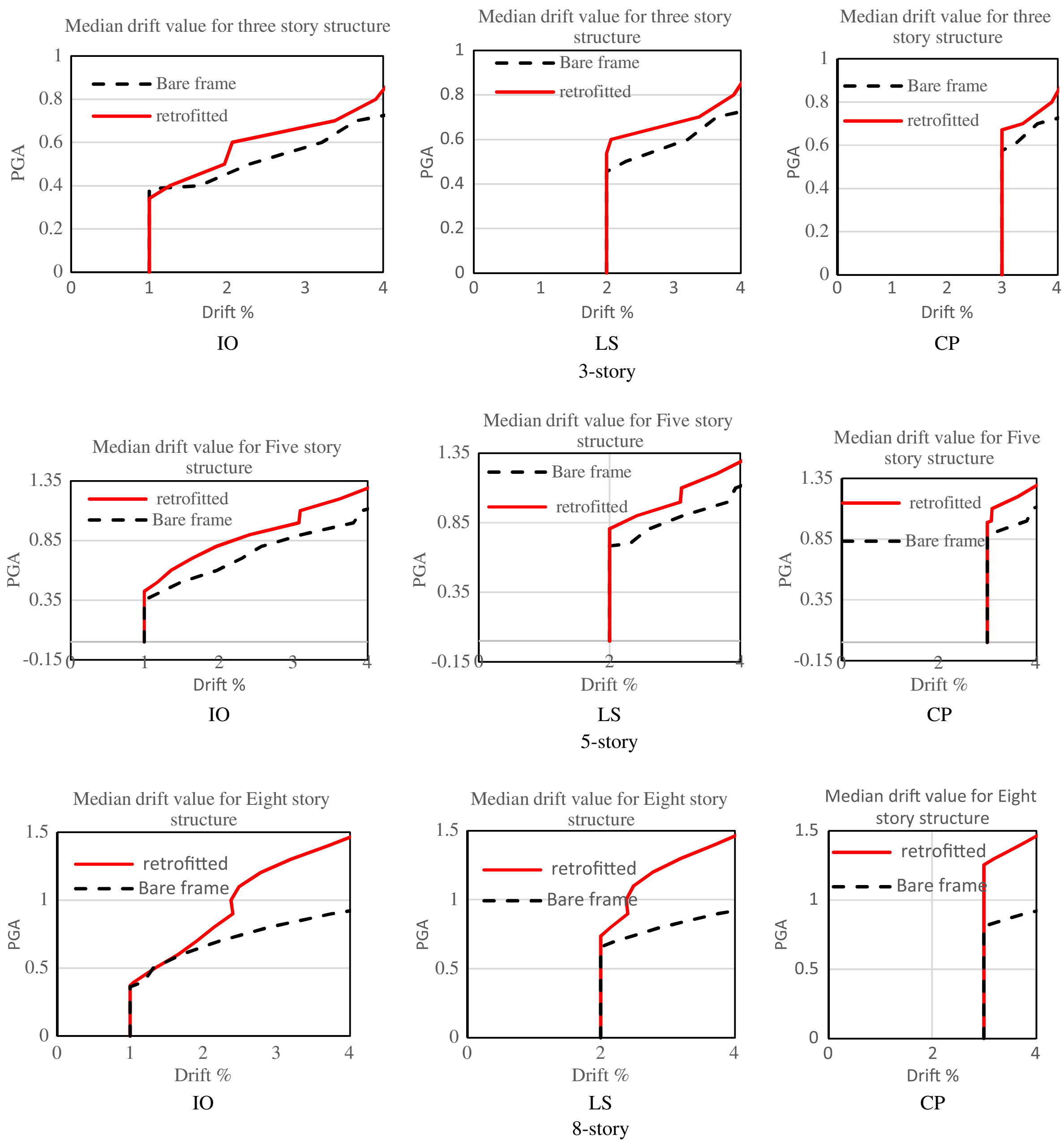

Fig. 17. MIDR versus spectral acceleration IDA curves indicating three damage states.

intensity measure until global dynamic instability is reached. A 4% interstory drift ratio is considered as the collapse limit state in which dynamic instability is encountered. Fig. 16 indicates the spectral acceleration versus MIDR curves of the model structures obtained using IDA before and after the retrofit. Each dot on the IDA curve represents the response for an earthquake scaled to the specific intensity level. Fig. 17 indicates the median MIDR versus spectral acceleration IDA curves of the model structures from a 1% up to a 4% drift ratio, which corresponds to the failure limit state. The seismic intensity for which 50% of the ground motion records lead to failure of the structure is called the median collapse capacity (Song et al. 2014). The median collapse capacities of the three-story frame before and after retrofit are observed to be 0.72 and 0.87 g, respectively. In the five-story structure, these values are 1.11 and 1.32 g, respectively, and in the eight-story structure, they are 0.91 and 1.48 g, respectively. Therefore, the proposed retrofit scheme is effective enough to increase the median collapse capacities of the three-, five-, and eight-story frames by 20.8%, 18.9%, and 62.6%, respectively, indicating that the improvement in the median collapse capacity of the eight-story structure is significantly larger than that of the three- or five-story ones. The median IDA curves also indicate that the effect of the retrofit is increasing with the severity of the limit state. For example, in the three-story structure, the increase in the intensity level is higher at interstory drift ratios of 2% (LS) and 3% (CP) compared with at a drift ratio of 1% (IO limit state). A similar observation is made for the five- and eight-story structures, indicating that the proposed retrofit is more effective for severe earthquakes than for medium earthquakes. In contrast, this improvement is more pronounced in the eight-story structure than the three- and five-story cases.

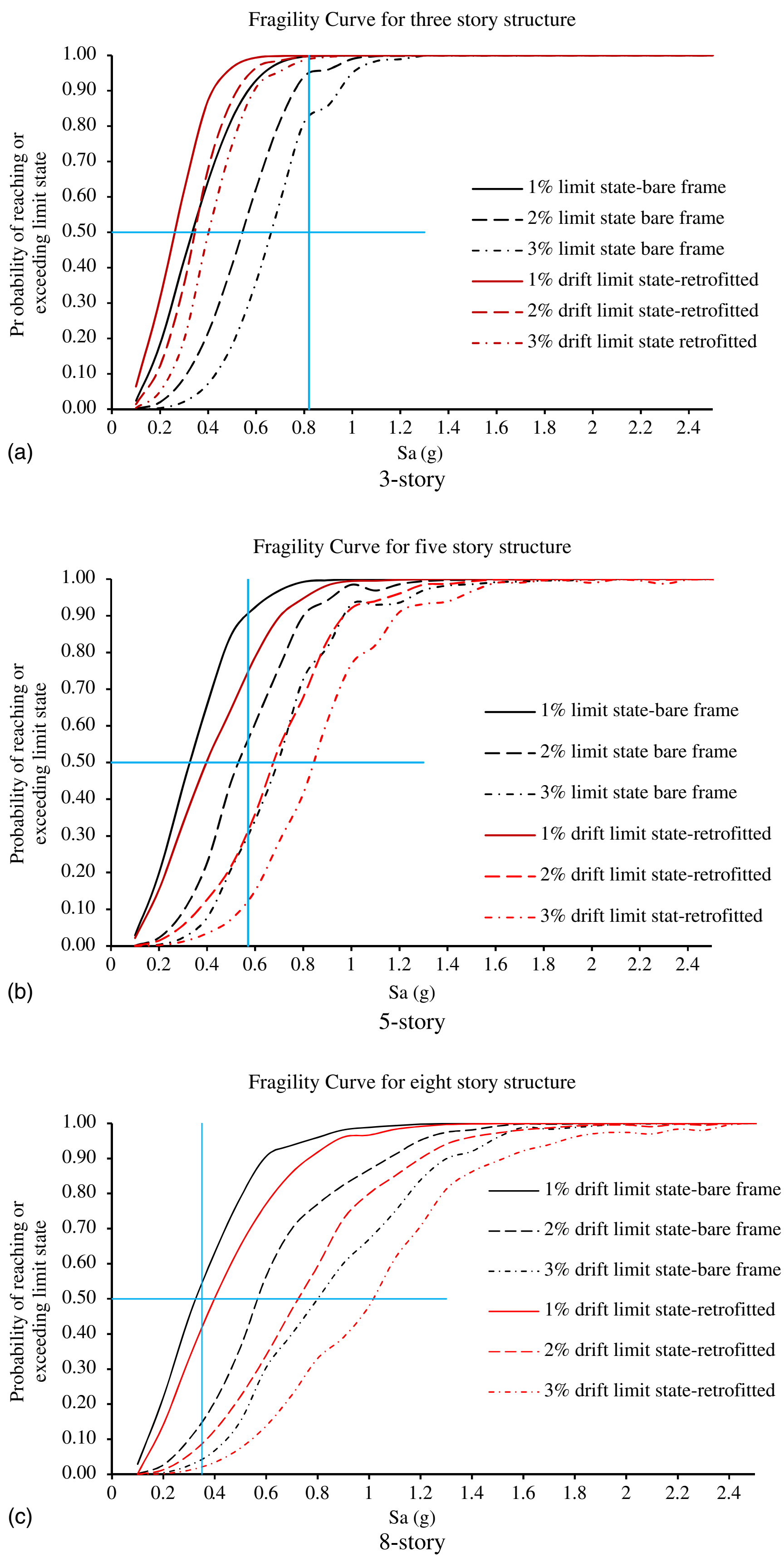

Fig. 18. Comparative fragility curves for bare and retrofitted frames at three damage states: (a) IO = 1.0%; (b) LS = 2.0%; and (c) CP = 3.0%.

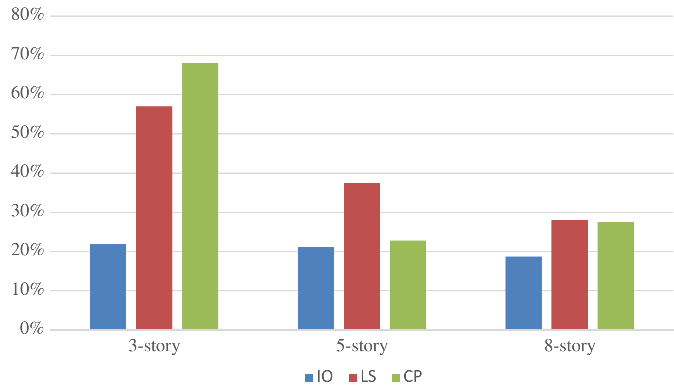

Fig. 19. Percentage increase of spectral acceleration at median probability of each limit state.

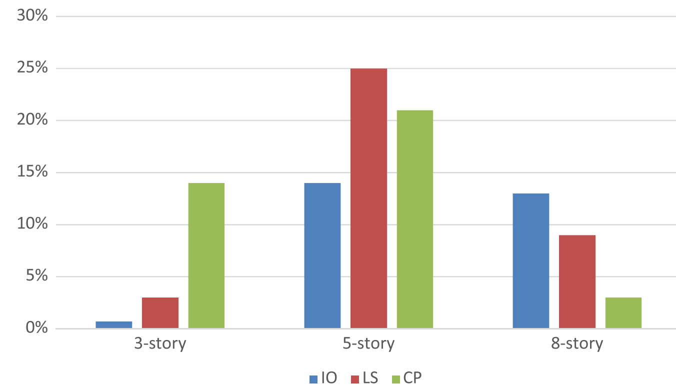

Fig. 20. Percentage decrease in probability of reaching limit states at model spectral acceleration.

Evaluation of Damage State Probabilities

The probability of a structure reaching a given damage state can be described using seismic fragility curves. These curves relate the seismic measure intensity with the probability that the structural capacity is less than the seismic demand for a specific limit state. This conditional probability lognormal cumulative distribution function can be given as (Celik and Ellingwood 2009)

$$P[C < D@SI = x] = 1 - \Phi\frac{\ln(\hat{C}/\hat{D})}{\beta_{TOT}} \tag{7}$$

where C = structural capacity; D = structural demand; SI = seismic intensity hazard; $\Phi[.]$ = standard normal probability integral; $\hat{C}$ = median structural capacity for a specific limit state; $\hat{D}$ = median structural demand; and β_{TOT} = total system collapse uncertainty, which is taken to be 0.6 using the FEMA P695 (FEMA 2009) recommendation.

Fig. 18 provides the comparative fragility curves for the bare and retrofitted model structures at IO, LS, and CP damage states, which corresponds to MIDR of 1%, 2%, and 3%, respectively. In Fig. 18, the horizontal line indicates the 50% probability of reaching or exceeding the limit states. In the three-story structure, the spectral acceleration at the median probability of reaching the limit states increases by 0.06, 0.20, and 0.27 g for the IO, LS, and CP limit states, respectively. In the five-story model, these values are 0.07, 0.15, and 0.16 g, respectively, and in the eight-story model, these values are 0.06, 0.16, and 0.22 g, respectively. Fig. 19 indicates a percentage increase in the spectral acceleration at the median probability of reaching each limit state, for which it is observed that the improvement in the spectral acceleration at the median probability of the LS and CP limit state is greater than that of the IO limit state in all model structures. In Fig. 18, the vertical lines indicate the average spectral acceleration of the structures before and after retrofit from the design spectrum corresponding to the natural period, which is 0.82, 0.57, and 0.35 g, respectively, for the three-, five-, and eight-story structures.

Fig. 20 provides the percentage decrease in the probability of reaching the limit states before and after the retrofit. To be noticed is that, in the three-story model, the probability of reaching LS and CP limit states at the design level spectral acceleration decreases by 3%, and 14%, respectively. However, no effect is noticed in the probability of the IO limit state. In the case of the five-story model, the probability of reaching IO, LS, and CP limit states at the design level spectral acceleration decreases by 14%, 25%, and 21%, respectively. In the eight-story model, the decrease is found to be 13%, 9%, and 3%, respectively. The effect of the retrofit is most significant in the reduction of the probability of reaching the IO and LS limit states for the five- and eight-story models. However, the reduction in the probability of reaching the CP limit state is most pronounced in the retrofit of the three- and five-story models.

Conclusion

In this study, the seismic retrofit effect of the self-centering PC frames was investigated through the cyclic loading test of a one-story RC frame and the fragility analysis of the analysis model structures. According to the test results, the maximum strength of the test specimen increased by 40% after the seismic retrofit. The lateral displacement at failure also increased as a result of the retrofit. The time history analyses results indicated that the SC-PC frames were effective in decreasing the maximum displacement and eliminating the residual drift. The IDA results indicated that the SC-PC retrofit scheme was effective in increasing the median collapse capacities of the three-, five-, and eight-story models by 20.8%, 18.9%, and 62.6%, respectively. The median IDA curves indicated that the increase in the intensity level due to retrofit increases with the severity of the limit state. Therefore, the increase in the intensity level associated with higher limit states, such as CP, is more pronounced than lower limit states, such as IO, for the proposed retrofit scheme. The fragility analysis results indicated that, for the three-story model, the largest decrease was observed in the probability of reaching the CP limit state with a value of 14%. In the five- and eight-story models, the largest decreases in seismic fragility were related to the IO limit state with a value of 25% and 13%, respectively. In terms of seismic fragility, the proposed retrofit method turned out to be most effective in the five-story structure.

Acknowledgments

This research was carried out by research funding (Grant No. 19CTAP-C153076-01) of the Ministry of Land, Infrastructure and Transport, Land Transport Technology Promotion Research Project.

References

ACI (American Concrete Institute). 2013. *Guide for testing reinforced concrete structural elements under slowly applied simulated seismic loads*. ACI 374.2r-13. Farmington Hills, MI: ACI.

ACI (American Concrete Institute). 2014. *Building code requirements for structural concrete.* ACI 318-14. Farmington Hills, MI: ACI.

AISC. 2016. *Specification for structural steel buildings*. AISC-360. Chicago: AISC.

ASCE. 2013. *Seismic evaluation and retrofit of existing buildings*. ASCE/SEI 41-13. Reston, VA: ASCE.

ASCE. 2016. *Minimum design loads for buildings and other structures*. ASCE/SEI 7. Reston, VA: ASCE.

ATC (Applied Technology Council). 1996. *Seismic evaluation and retrofit of concrete buildings*. Rep. No. ATC 40. Redwood City, CA: ATC.

Bahrami, S., M. Madhkhan, F. Shirmohammadi, and N. Nazemi. 2017. "Behavior of two new moment resisting precast beam to column connections subjected to lateral loading." *Eng. Struct.* 132 (Feb): 808–821. https://doi.org/10.1016/j.engstruct.2016.11.060.

Bocchini, P., D. M. Frangopol, T. Ummenhofer, and T. Zinke. 2014. "Resilience and sustainability of civil infrastructure: Toward a unified approach." *J. Infrastruct. Syst.* 20 (2): 04014004. https://doi.org/10.1061/(ASCE)IS.1943-555X.0000177.

Buchanan, A. H., D. Bull, R. Dhakal, G. MacRae, A. Palermo, and S. Pampanin. 2011. *Base isolation and damage-resistant technologies for improved seismic performance of buildings*. Technical Rep. No. 2011-02 for the Royal Commission of Inquiry into Building Failure Caused by the Canterbury Earthquakes. Christchurch, New Zealand: Univ. of Canterbury.

Celik, O., and S. Sritharan. 2004. *An evaluation of seismic design guidelines proposed for precast concrete hybrid frame systems*. ISU-ERI-Ames Rep. No. ERI-04425. Ames, IA: Iowa State Univ. of Science and Technology.

Celik, O. C., and B. R. Ellingwood. 2009. "Seismic risk assessment of gravity load designed reinforced concrete frames subjected to Mid-America ground motions." *J. Struct. Eng.* 135 (4): 414–424. https://doi.org/10.1061/(ASCE)0733-9445(2009)135:4(414).

Dyanati, M., Q. Huang, and D. Roke. 2017. "Cost-benefit evaluation of self-centring concentrically braced frames considering uncertainties." *Struct. Infrastruct. Eng.* 13 (5): 537–553. https://doi.org/10.1080/15732479.2016.1173070.

Eldin, M. N., J. Kim, and J. Kim. 2018. "Optimum distribution of steel slit-friction hybrid dampers based on life cycle cost." *Steel Compos. Struct.* 27 (5): 633–646. https://doi.org/10.12989/scs.2018.27.5.633.

Englekirk, R. E. 2002. "Design-construction of the paramount—A 39-story precast prestressed concrete apartment building." *PCI J.* 47 (4): 56–71. https://doi.org/10.15554/pcij.07012002.56.71.

FEMA. 2009. *Quantification of building seismic performance factors*. FEMA P695. Washington, DC: FEMA.

Guerrini, G., J. I. Restrepo, M. Massari, and A. Vervelidis. 2008. "Seismic behavior of posttensioned self-centering precast concrete dual-shell steel columns." *J. Struct. Eng.* 141 (4): 04014115. https://doi.org/10.1061/(ASCE)ST.1943-541X.0001054.

Guo, T., L. L. Song, Z. Cao, and Y. Gu. 2016. "Large-scale tests on cyclic behavior of self-centering prestressed concrete frames." *ACI Struct. J.* 113 (6): 1263–1274.

Guo, T., L. L. Song, and G. D. Zhang. 2015. "Numerical simulation and seismic fragility analysis of self-centering steel MRF with web friction devices." *J. Earthquake Eng.* 19 (5): 731–751. https://doi.org/10.1080/13632469.2014.1003437.

Guo, T., Z. Xu, L. Song, L. Wang, and Z. Zhang. 2017. "Seismic resilience upgrade of rc frame building using self-centering concrete walls with distributed friction devices." *J. Struct. Eng.* 143 (12): 04017160. https://doi.org/10.1061/(ASCE)ST.1943-541X.0001901.

Huang, L., Z. Zhou, Z. Zhang, and X. Huang. 2018. "Seismic performance and fragility analyses of self centering prestressed concrete frames with infill walls." *J. Earthquake Eng.* 1–31. https://doi.org/10.1080/13632469.2018.1526142.

Hutt, C. M., I. Almufti, M. Willford, and G. Deierlein. 2016. "Seismic loss and downtime assessment of existing tall steel-framed buildings and strategies for increased resilience." *J. Struct. Eng.* 142 (8): C4015005. https://doi.org/10.1061/(ASCE)ST.1943-541X.0001314.

Kim, J., and S. Bang. 2003. "Optimum distribution of added VED for mitigation of torsional responses of plan-wise asymmetric structures." *Eng. Struct.* 24 (10): 257–269. https://doi.org/10.1016/S0141-0296(02)00046-9.

Kim, J., J. Park, and S. D. Kim. 2009. "Seismic behavior factors of buckling-restrained braced frames." *Struct. Eng. Mech.* 33 (3): 261–284. https://doi.org/10.12989/sem.2009.33.3.261.

Lee, S. K., J. H. Park, B. W. Moon, K. W. Min, S. H. Lee, and J. Kim. 2008. "Design of a bracing-friction damper system for seismic retrofitting." *Smart Struct. Syst.* 4 (5): 685–696. https://doi.org/10.12989/sss.2008.4.5.685.

Mattock, A. H. 1979. "Flexural strength of prestressed concrete sections by programmable calculator." *PCI J.* 24 (1): 32–54. https://doi.org/10.15554/pcij.01011979.32.54.

Morgen, B. G., and Y. C. Kurama. 2008. "Seismic response evaluation of posttensioned precast concrete frames with friction dampers." *J. Struct. Eng.* 134 (1): 132–145. https://doi.org/10.1061/(ASCE)0733-9445(2008)134:1(132).

Naeem, A., and J. Kim. 2018a. "Seismic performance evaluation of a spring viscous damper cable system." *Eng. Struct.* 176 (Dec): 455–467. https://doi.org/10.1016/j.engstruct.2018.09.055.

Naeem, A., and J. Kim. 2018b. "Seismic retrofit of a framed structure using damped cable systems." *Steel Compos. Struct.* 29 (3): 287–299. https://doi.org/10.12989/scs.2018.29.3.287.

Nour Eldin, M., A. Naeem, and J. Kim. 2019. "Seismic retrofit of a structure using self-centring precast concrete frames with enlarged beam ends." *Mag. Concr. Res.* 1–16. https://doi.org/10.1680/jmacr.19.00012.

Palermo, A., and S. Pampanin. 2008. "Enhanced seismic performance of hybrid bridge systems: Comparison with traditional monolithic solutions." *J. Earthquake Eng.* 12 (8): 1267–1295. https://doi.org/10.1080/13632460802003819.

PEER (Pacific Earthquake Engineering Research). 2017. "Center: NGA database." November 8, 2017. http://peer.berkeley.edu/nga/.

Priestley, M. N. 1991. "Overview of PRESSS research program." *PCI J.* 36: 50–57. https://doi.org/10.15554/pcij.07011991.50.57.

Priestley, M. N. 1996. "The PRESSS program: Current status and proposed plans for phase III." *PCI J.* 41 (2): 22–40. https://doi.org/10.15554/pcij.03011996.22.40.

Priestley, N. M. J., S. Sritharan, J. R. Conley, and S. Pampanin. 1999. "Preliminary results and conclusions from the PRESSS five-story precast concrete test building." *PCI J.* 44 (6): 42–67. https://doi.org/10.15554/pcij.11011999.42.67.

Qiu, C., and S. Zhu. 2017. "Shake table test and numerical study of self-centering steel frame with SMA braces." *Earthquake Eng. Struct. Dyn.* 46 (1): 117–137. https://doi.org/10.1002/eqe.2777.

Rahman, M. A., and S. Sritharan. 2007. "Performance-based seismic evaluation of two five-story precast concrete hybrid frame buildings." *J. Struct. Eng.* 133 (11): 1489–1500. https://doi.org/10.1061/(ASCE)0733-9445(2007)133:11(1489).

Sap2000. 2015. *Analysis reference manual, version 18*. Berkeley, CA: Computer and Structures.

Song, L. L., T. Guo, Y. Gu, and Z. L. Cao. 2015. "Experimental study of a self-centering prestressed concrete frame subassembly." *Eng. Struct.* 88 (Apr): 176–188. https://doi.org/10.1016/j.engstruct.2015.01.040.

Song, R., Y. Li, and J. W. van de Lindt. 2014. "Impact of earthquake ground motion characteristics on collapse risk of post-mainshock buildings considering aftershocks." *Eng. Struct.* 81 (Dec): 349–361. https://doi.org/10.1016/j.engstruct.2014.09.047.

Whittaker, A. S., V. V. Bertero, C. L. Thompson, and L. J. Alonso. 1991. "Seismic testing of steel plate energy dissipation devices." *Earthquake Spectra* 7 (4): 563–604. https://doi.org/10.1193/1.1585644.

Wiebe, L., and C. Christopoulos. 2014. "Controlled rocking systems for enhanced seismic resilience: State of the art." In *Sustainable development of critical infrastructure*, 496. Reston, VA: ASCE.